Application of an array of four phase-detection probe sensors to hydraulic jumps at large Reynolds numbers

Hang Wang[1] **and Hubert Chanson**[2]*

[1] *The University of Queensland*
School of Civil Engineering, Brisbane QLD 4072, Australia
hang.wang@uqconnect.edu.au

[2] *The University of Queensland*
School of Civil Engineering, Brisbane QLD 4072, Australia
h.chanson@uq.edu.au

Abstract

The measurement of turbulent velocity is difficult in hydraulic jumps with relatively high Reynolds numbers because of the presence of entrained air bubbles. This study presents a method aimed to characterise the three-dimensional velocity field in hydraulic jumps using a four-sensor phase-detection probe array. Besides the longitudinal velocity and turbulence intensity that were measured for both positive and negative velocity flow regions, a characteristic instantaneous transverse velocity component was derived together with a measure of its fluctuations. The transverse velocity component characterised the three-dimensional nature of turbulent structures. Although the time-averaged flow pattern was two-dimensional and the average transverse velocity was zero, the transverse velocity fluctuation was found to be one order of magnitude smaller than the longitudinal velocity fluctuation.

Keywords: Phase-detection probe array, hydraulic jumps, velocity measurements, turbulence intensity, Reynolds stresses

1. Introduction

A hydraulic jump is a sudden transition from a supercritical flow to a subcritical flow [1],[19]. It is commonly encountered in natural waterways and hydraulic structures with a rapid expansion of flow cross-sectional area or presence of barrier structures [1],[2]. Figure 1A shows a hydraulic jump forming at the downstream foot of a weir, with the curved impingement perimeter highlighted by depth discontinuity. Figure 1B illustrates an experimental hydraulic jump in a horizontal rectangular channel. In Figure 1B, large-scale vortical structures are visualised by the air bubbles entrained at the jump toe and through the roller surface. The bubbles are advected downstream and ultimately de-aerated in the tailwater.

A hydraulic jump flow is highly turbulent and highly aerated. The characterisation of turbulence is of significant importance for the understanding of flow regimes and its practical applications, e.g. to enhance fluid mixing and energy dissipation. However, the presence of air bubbles adversely affects the use of most traditional velocity measurement instruments such as LDV, ADV and PIV. These instruments are designed for monophase flow, and their application in hydraulic jump studies was restricted to very weak jumps with a low aeration level [3],[5],[6],[7]. In the past decades, the largest number of and most successful air-water flow measurements in hydraulic jumps were conducted with intrusive phase-detection conductivity probes. The needle-shaped probe sensor detects the air-water interfaces based upon the different electrical resistivity between air and water [4],[8],[9]. Besides the local void fraction and bubble count rate measured by a single needle sensor, the simultaneous sampling of two sensors of a dual-tip probe enables derivation of time-averaged air-water interfacial velocity and corresponding turbulence intensity.

Based on this technique, a new configuration of phase-detection probe array was applied in the present study to investigate the three-dimensional flow structure and turbulence field. The three-dimensional structures in hydraulic jump received limited attention partially because the time-averaged flow pattern can be reasonably treated as two-dimensional. However, people did observe instantaneous three-dimensional structures on the free-surface and in the roller [2],[10],[11],[12]. Herein an array of four phase-detection sensors was used to detect velocity components in a horizontal plane. A characteristic instantaneous transverse velocity component and the corresponding transverse velocity fluctuation were derived. Besides the normal probe orientation with the sensors aligned against the inflow direction, the probes were reversed in the upper free-surface recirculation region to examine the impact of the reversing flow on air-water interface detection.

(A) Hydraulic jump at the toe of Chinchilla weir (Australia)

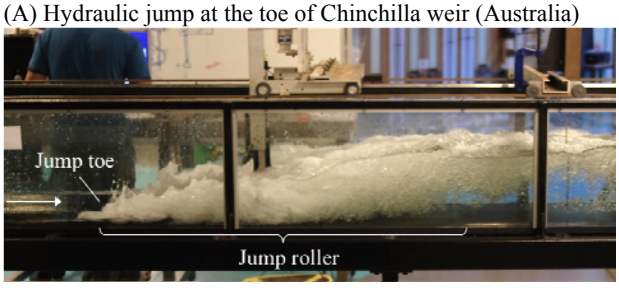

(B) Hydraulic jump in horizontal rectangular channel. Flow from left to right. Flow rate: 0.0347 m^3/s; channel width: 0.5 m; inflow depth: 0.0206 m; inflow length: 0.83 m; inflow Froude number: 7.5; Reynolds number: 68,000.

Figure 1: Hydraulic jumps in hydraulic structure and laboratory.

* Support from grant ARC DP120100481 is gratefully acknowledged.

2. Physical facility and instrumentation

The experimental channel was a 3.2 m long, 0.5 m wide rectangular channel built with a smooth, horizontal HDPE bed and 0.4 m high glass sidewalls (Fig. 1B). Water was discharged into the channel from an upstream head tank. The head tank was equipped with a series of baffles and flow straighteners, followed by an undershoot gate, of which the rounded edge induced a horizontal impinging flow without contraction. The position of the hydraulic jump was controlled by an overshoot gate located at the downstream end of the channel. The flow rate was measured with a Venturi meter in the supply pipeline that fed the head tank, with an expected accuracy of ±2%.

The clear water depths were measured with a pointer gauge. The air-water flow measurements were conducted using a series of phase-detection conductivity probes. Figure 2A shows two dual-tip probes side by side, forming a four-tip sensor array, as sketched in Figure 2B. Each dual-tip probe was equipped with two needle sensors (Ø = 0.25 mm) of different lengths. All sensors (numbered from 1 to 4 in Fig. 2B) were located within the same x-z plane. The longitudinal distance between the leading and trailing sensor tips was 6.5 mm, and the transverse separation distance between two leading tips was 10 mm (Fig. 2B). All sensors were excited simultaneously and sampled herein at 20 kHz for 45 s at each single measurement location. The vertical position of the probes was monitored using a Mitutoyo^{TM} digimatic scale unit with an accuracy of ±0.01 mm.

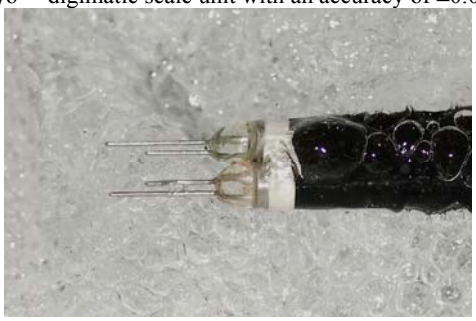

(A) Photograph of probe array next to roller surface

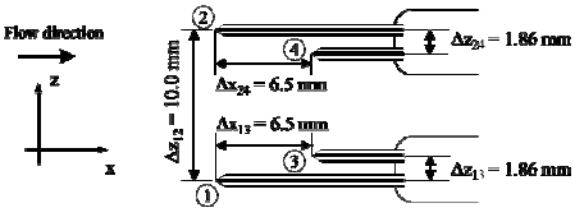

(B) Sketch of probe array configuration in top view

Figure 2: Four-tip phase-detection probe array. Views in elevations.

3. Data processing

Post-processing and analyses of the phase-detection probe signals provided a large amount of information on the air-water flow and air-water turbulence characteristics. Considering the probe configuration in Figure 2B, let us define $R_{ij}(\tau)$ as the normalised cross-correlation function between the signals of sensors i and j, where τ is the signal time lag and i,j = 1,2,3,4. For i = j, $R_{ii}(\tau)$ is the auto-correlation function of the signal of sensor i. Let us further define the characteristic time lag T_{ij} satisfying $R_{ij}(\tau=T_{ij}) = (R_{ij})_{max}$, with $(R_{ij})_{max}$ the maximum cross-correlation coefficient, and the correlation time scale t_{ij}:

$$t_{ij} = \int_{\tau(R_{ij}=(R_{ij})_{max})}^{\tau(R_{ij}=0)} R_{ij}(\tau) \times d\tau \quad (1)$$

The time-averaged velocity of the air-water interfaces travelling between sensor tips i and j may be estimated as

$$V_{ij} = \frac{\sqrt{\Delta x_{ij}^{\ 2} + \Delta z_{ij}^{\ 2}}}{T_{ij}} \quad (2)$$

where Δx_{ij} and Δz_{ij} are the longitudinal and transverse distances between sensors i and j. The turbulent velocity fluctuation may be derived as

$$v_{ij}' = \frac{\sqrt{2 \times \left(\Delta x_{ij}^{\ 2} + \Delta z_{ij}^{\ 2}\right)}}{\sqrt{\pi} \times T_{ij}^{\ 2}} \times \sqrt{\left(\frac{t_{ij}}{(R_{ij})_{max}}\right)^2 - t_{ii}^{\ 2}} \quad (3)$$

Equation (3) is based upon the work of Chanson & Toombes [13] and Felder & Chanson [14]. It is valid for a truly random detection of an infinitely large number of air-water interfaces. For the probe array configuration in Figure 2, six characteristic velocities are obtained altogether, following the relationships:

$$V_{13} \approx V_{24} \approx V_x \quad (4)$$

$$V_{12} \approx V_{34} \approx V_z \quad (5)$$

$$V_{23} = \sqrt{V_{13}^{\ 2} + V_{23}^{\ 2}} \approx V_{14} = \sqrt{V_{24}^{\ 2} + V_{12}^{\ 2}} \approx \sqrt{V_x^{\ 2} + V_z^{\ 2}} \quad (6)$$

where V_x and V_z are the time-averaged interfacial velocity components in the longitudinal and horizontal transverse directions respectively. For the velocity fluctuations, the following relationships may hold:

$$v_{13}' \approx v_{24}' \approx v_x' \quad (7)$$

$$v_{12}' \approx v_{34}' \approx v_z' \quad (8)$$

$$v_{23}' = \sqrt{v_{13}'^2 + v_{12}'^2 + 2 \times \left(v_{13} \times v_{12}\right)'}$$

$$\approx v_{14}' = \sqrt{v_{24}'^2 + v_{12}'^2 + 2 \times \left(v_{24} \times v_{12}\right)'} \quad (9)$$

In practice, for signals consisting of a sufficiently large amount of sample points, the cross-correlation function $R_{12}(\tau)$ between the leading tip signals exhibits maximum at zero time lag: i.e. $T_{12} \approx 0$. This corresponds to the detection of the longitudinal interface convection at the same longitudinal positions ($\Delta x_{12} = 0$). For a relatively long sampling duration (e.g. 45 s), the statistical analysis hardly gives any information of the instantaneous transverse motion in a quasi-two-dimensional flow. On the other hand, a small signal segment may be able to reflect some instantaneous transverse interface motion. Such a time interval should be comparable to or slightly larger than the time scale of the transverse interface motion. While a too small time interval might not cover a sufficient amount of air-water interfaces, a too large interval would contain too many interfaces belonging to various motions and give an average transverse velocity being infinitely large ($T_{12} \approx 0$ in Eq. (2)).

In the present study, a time interval 0.2 s was selected, after an initial sensitivity analysis, to investigate the transverse interfacial motion. Figure 3 shows a typical cross-correlation function between two 0.2 s leading tip signal segments. The correlation coefficient R_{12} is plotted as a function of the ratio of transverse sensor separation Δz_{12} to time lag τ. The peaks in the correlation function might indicate some characteristic transverse velocities. The local maximum correlation coefficient

was picked for every 0.5 m/s velocity bin between $\Delta z_{12}/\tau$ = -5 and 5 m/s, as marked by arrows in Figure 3. For the entire 45 s signal data set, a total of fifty non-overlapping 0.2 s signal segments were analysed, giving 120 to 300 characteristic velocities. The probability of these characteristic transverse velocities followed closely a normal distribution. Some small transverse velocities were only recorded when the sensor separation distance Δz_{12} was small because of the small size or short 'lifetime' of the bubbly structures moving or oscillating transversely. These small turbulent structures were not detected by both sensors when Δz_{12} was larger than their largest transverse displacement. For a given Δz_{12}, the median transverse velocity amplitude $|V_z|$ was considered. It reflected a typical instantaneous velocity or velocity fluctuation magnitude between the given distance Δz_{12}. The value of $|V_z|$ was a function of the sensor separation distance Δz_{12}. A larger distance Δz_{12} gave a higher characteristic transverse velocity $|V_z|$. It is important to note that the results in the present study were obtained for a transverse sensor separation Δz_{12} = 10 mm and a time interval selection of 0.2 s.

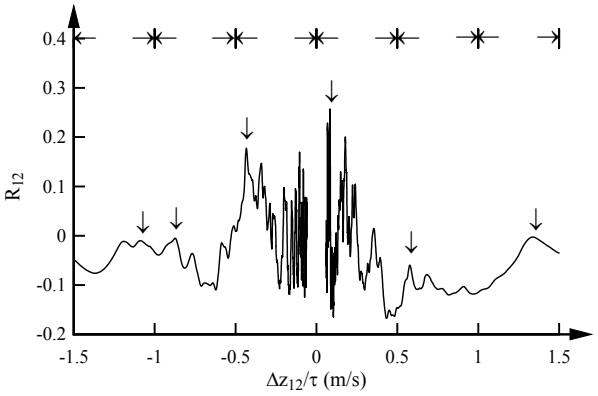

Figure 3: Cross-correlation function between two 0.2 s leading tip signals as a function of the ratio of transverse tip separation to time lag; Arrows indicating the maximum peaks in every 0.5 m/s interval.

Table 1: Experimental flow conditions

Q [m^3/s]	h [m]	x_1 [m]	d_1 [m]	V_1 [m]	Fr_1 [-]	Re [-]
0.0347	0.02	0.83	0.0206	3.37	7.5	6.8×10^4
0.0705	0.03	1.25	0.033	4.27	7.5	1.4×10^5

Note: Q: flow rate; h: upstream gate opening; x_1: longitudinal jump toe position; d_1: inflow depth; V_1: average inflow velocity; Fr_1: inflow Froude number; Re: Reynolds number

4. Experimental flow conditions

The physical measurements were performed for two hydraulic jumps with the same inflow Froude number Fr_1 = 7.5 but different inflow aspect ratios h/W = 0.04 and 0.06, where h is the upstream gate opening and W is the channel width (W = 0.5 m). The corresponding Reynolds numbers were Re = 6.8×10^4 and 1.4×10^5 respectively. The longitudinal jump toe position x_1 was set at x_1 = 41.5×h downstream of the gate. Such an inflow length corresponded to partially-developed inflow conditions. Detailed air-water measurements were undertaken at five vertical cross-sections on the channel centreline at $x\text{-}x_1$ = 4.15×h, 8.35×h, 12.5×h, 18.75×h and 25×h. The experimental flow conditions are summarised in Table 1.

5. Velocity and turbulence intensity in longitudinal direction

For an inflow Froude number Fr_1 = 7.5, the hydraulic jump was characterised by a marked jump roller (Fig. 1B). While the impinging flow sustained a relatively high velocity beneath the roller, flow recirculation took place next to the free-surface, with spray and splashing projected in air [12],[20]. A shear layer formed between the bottom boundary layer ($V_x > 0$) and the upper reversing flow ($V_x < 0$). A considerable amount of air was entrained into the shear layer at the jump toe. The entrained air bubbles were carried in large-size vortices in the shear layer and diffused during the downstream advection.

The time-averaged longitudinal velocity V_x/V_1 was calculated using Equation (2) with $\Delta z_{ij} \approx 0$. The four-tip probe array gave V_x data at two transverse locations: z = 0 ($V_x = V_{13}$) and z = 10 mm ($V_x = V_{24}$). The results are presented in Figure 4A for Fr_1 = 7.5, Re = 6.8×10^4 at $(x\text{-}x_1)/d_1$ = 4.03 and in Figure 4B for Fr_1 = 7.5, Re = 1.4×10^5 at $(x\text{-}x_1)/d_1$ = 22.73. Further we use $V_x(+)$ and $V_x(-)$ to denote respectively the results obtained with normal probe position where the sensors pointed upstream and reversed probe orientation with the sensors pointing downstream. The latter setup was applied in the upper roller region to minimise the interference of probe support structure to the measurements in the reversing flow. Figure 4 also includes some water-phase velocity data collected for the same flow conditions using Prandtl-Pitot tube next to the channel bed. The time-averaged void fraction C is also plotted for reference.

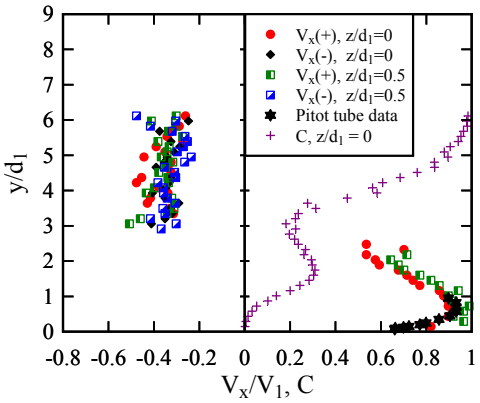

(A) Fr_1 = 7.5, Re = 6.8×10^4, $(x\text{-}x_1)/d_1$ = 4.03

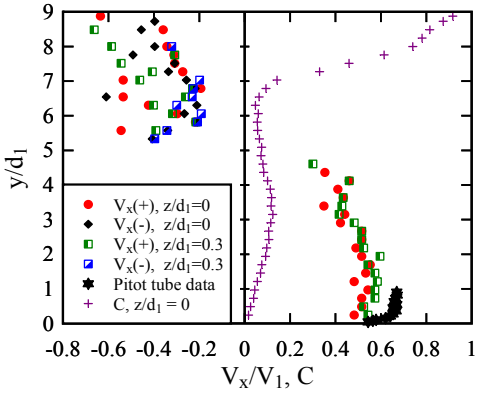

(B) Fr_1 = 7.5, Re = 1.4×10^5, $(x\text{-}x_1)/d_1$ = 22.73

Figure 4: Time-averaged longitudinal interfacial velocity measured at z = 0 and z = 10 mm with normal and reversed probe orientation in the recirculation region – Comparison with Prandtl-Pitot tube data next to channel bed and time-averaged void fraction.

In Figure 4, the time-averaged longitudinal velocity showed a positive velocity region in the lower part of the roller and a negative velocity region in the upper part of the roller. A boundary layer can be seen developing next to the channel bed. Meaningful velocity data were absent in the transitional area between the positive and negative velocity regions because the intrinsic limitation of cross-correlation technique. The raw signal suggested frequent switches of instantaneous velocity direction in this area, yielding a small mean velocity $V_x \sim 0$ but large turbulence intensity $Tu_x = v_x'/V_x$ [15]. The velocities measured at slightly separated transverse positions (z = 0 & 10 mm) were almost identical, confirming that the mean flow was quasi-two-dimensional. Comparison between the data recorded with opposite probes orientations did not show major difference, though a close check of the recirculation velocity distributions suggested a lesser data scatter for the results given by the reversed probe sensors. The finding implied a relatively limited impact of the probe orientation on velocity measurement in the recirculation region; the data scatter caused by the probe interference might be acceptable even for a reversing flow. However, this conclusion only applies to the free-surface reversing flow where the velocity was moderate to small and the gravity force dominated rather than shear stress.

In the lower flow region close to the invert, the interfacial velocity data measured with the phase-detection probe were close to the water-phase velocity recorded by Prandtl-Pitot tube in the high-velocity lower shear region, although some difference was observed after major flow deceleration and de-aeration at downstream end of the roller (Fig. 4B).

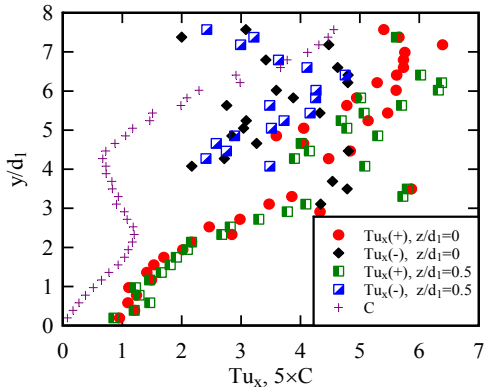

Figure 5: Turbulence intensity measured at z = 0 and 10 mm with normal and reversed probe orientation in the recirculation region – Flow conditions: $Fr_1 = 7.5$, $Re = 6.8\times10^4$, $(x-x_1)/d_1 = 12.14$.

The turbulence intensity $Tu_x = v_x'/V_x$ was derived from Equation (3) and the results are shown in Figure 5 for a selected cross-section. The overall data distributions were consistent with previous studies using similar instrumentation [16],[17]. Namely, in the lower turbulent shear flow, the turbulence intensity increased with increasing elevation from the bottom, while it decreased along the longitudinal direction as the turbulence was dissipated streamwise. The magnitude of Tu_x was found mainly between 1 and 2.5 in this region. Such values were high for random velocity turbulence, even with consideration to the large Froude and Reynolds numbers. But the contribution of slower flow motions associated with the fluctuating nature of hydraulic jump could not be neglected as demonstrated by Wang et al. [12]. In the recirculation region next to the free-surface, the turbulence intensities were high with large data scatter, because of the effects of jump translations and free-surface deformations. A comparison between the results given by opposite probe orientations ($Tu_x(+)$ and $Tu_x(-)$) suggested that the intrusive probe disturbance in the reversing flow also contributed to some extend to an overestimate of velocity fluctuation. The findings indicated that the wake effects induced by the probe support structures were negligible for the measurement of time-averaged velocity but should not be neglected for the estimate of velocity fluctuation.

6. Four-point air-water flow measurements and transverse velocity fluctuations

6.1. Characteristic transverse velocity component

The simultaneous four-point air-water flow measurements using two dual-tip phase-detection probes (Fig. 2) allowed for the derivation of turbulent characteristics in the transverse direction. The method to determine the characteristic transverse velocity component $|V_z|$ is described in Section 3. Figure 6 presents the dimensionless transverse velocity $|V_z|/V_1$ for the same flow conditions and at the same positions as for the data presented in Figure 4. In Figure 6, the transverse velocity data are compared with the longitudinal component V_x/V_1. Herein $|V_z|$ is a median transverse velocity amplitude. The instantaneous transverse velocity could be in either positive (+z direction) or negative (-z direction), the average being zero. Figure 6 shows similar profiles between the transverse and longitudinal velocity components in the shear flow and recirculating flow regions respectively. In the shear region with positive velocity ($V_x > 0$), the transverse velocity amplitude $|V_z|$ reached a maximum at the upper edge of boundary layer. In the recirculation region ($V_x < 0$), $|V_z|$ was relatively uniform; the results were almost independent of the probe elevation and phase-detection probe orientation ($|V_z(+)| \approx |V_z(-)|$). The ratio of transverse to longitudinal velocity amplitudes was typically between $|V_z|/|V_x| = 0.4$ and 0.5. That is, for a physical measurement with length scale $\sim10^{-2}$ m and a time scale no larger than 0.2 s, a typical instantaneous transverse motion of air-water interfaces was about half of the time-averaged longitudinal velocity.

The derivation process implied that $|V_z|$ was a function of both the sensor separation distance Δz_{12} and the duration of the signal segment (herein 0.2 s for $\Delta z_{12} = 10$ mm). For a selected signal duration, an increase in sensor separation distance yielded a larger characteristic transverse velocity since it performed a filtering on the small velocity components. A consideration of integral turbulent length scale suggested a typical transverse dimension of the bubbly-vortical structures in an order of $0.1\times d_1$ to $1.0\times d_1$ [12], comparable to the present value adopted for Δz_{12}. A larger sensor separation was thought to hardly capture the transverse motion of a coherent structure thus the data might be of less interest. By comparison, the measurement of time-averaged longitudinal velocity was independent of the longitudinal sensor separation Δx_{13} and Δx_{24}, within 2.5 mm < Δx < 29.7 mm for the present experimental flow conditions.

Equation (6) was checked by comparing the velocity vectors $(V_x^2+V_z^2)^{1/2}$ with the velocities V_{23} (or V_{14}) directly measured between the corresponding sensors. Figure 7 illustrates the results, showing that the calculation and measurement results were of the same order of magnitude. A significant deviation from the 1:1 line is seen, especially in the reversing flow region. This could be attributed to the scatter of velocity data measured

between probe sensors that were not aligned along the flow direction.

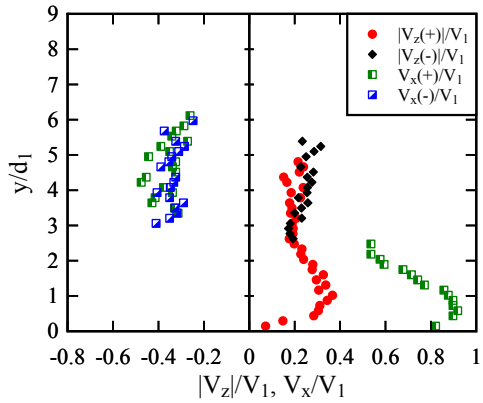

(A) $Fr_1 = 7.5$, $Re = 6.8\times10^4$, $(x-x_1)/d_1 = 4.03$

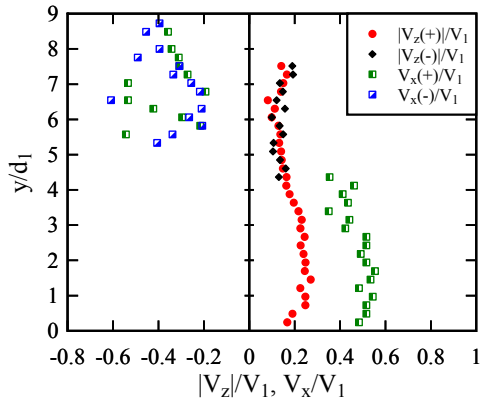

(B) $Fr_1 = 7.5$, $Re = 1.4\times10^5$, $(x-x_1)/d_1 = 22.73$

Figure 6: Characteristic instantaneous transverse velocity component $|V_z|/V_1$ – Comparison with the longitudinal velocity component V_x/V_1.

6.2. Transverse turbulent fluctuations

The velocity standard deviation $v_z' = v_{12}'$ was calculated using Equation (3) for the given characteristic transverse velocity $|V_z| = |V_{12}|$. Figure 8 shows the results at a cross-section in the form of relative velocity fluctuation to the local time-averaged longitudinal velocity $v_{12}'/|V_x|$. The longitudinal velocity fluctuation $Tu_x = v_{13}'/|V_x|$ and $v_{24}'/|V_x|$ are included for comparison. The data indicated relative transverse velocity fluctuations $v_{12}'/|V_x|$ typically between 0.02 and 0.5, compared to the longitudinal turbulence intensities mostly larger than 1. This was quantitatively comparable to the findings of Resch & Leutheusser [18] who measured water-phase turbulence intensities using a double V-shaped hot-film probe for $Fr_1 = 6$. At different longitudinal positions, the data also showed decreasing magnitude of transverse velocity turbulence with increasing distance from the jump toe.

Equation (9) holds for a quasi-two-dimensional flow, where the terms $v_{23}'^2$ and $v_{14}'^2$ are proportional to a combination of normal and tangential Reynolds stresses. Thus the results might provide an indirect means to estimate the tangential Reynolds stress component:

$$(v_x \times v_z)' \approx \frac{1}{2} \times \left(v_{23}'^2 - v_x'^2 - v_z'^2\right) \qquad (10)$$

where v_{23}' (or v_{14}') needs to be measured between two phase-detection sensors. Figure 9 presents the dimensionless Reynolds stresses for the corresponding velocity fluctuations. The present data showed dimensionless normal Reynolds stress larger than 1 in the longitudinal direction, and typically smaller than 0.1 in the transverse direction. The tangential Reynolds stress was of the same order of magnitude as the longitudinal normal stress. The tangential stress data yielded unusually large values because, in Equation (10), the terms v_{23}' (or v_{14}') measured apart from the main flow direction were sometimes large, scattered and physically meaningless. For comparison, Resch & Leutheusser [18] measured the water-phase tangential stress $(v_x \times v_z)'/V_1^2$ in the order of 10^{-2}, and the normal stress $v_x'^2/V_1^2$ in the order of 10^{-1}.

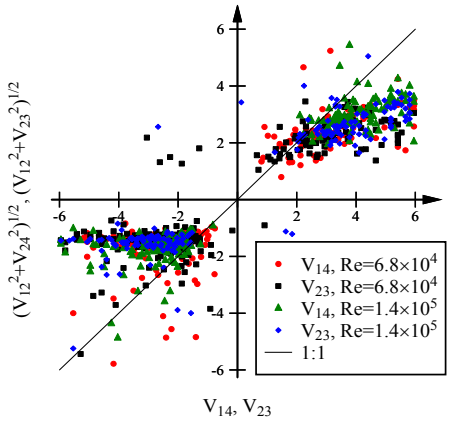

Figure 7: Comparison between velocity vectors measured with phase-detection sensors and calculated with Equation (6).

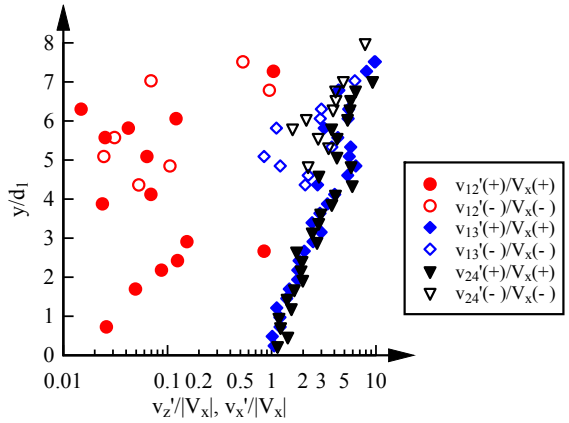

Figure 8: Transverse and longitudinal velocity fluctuations.

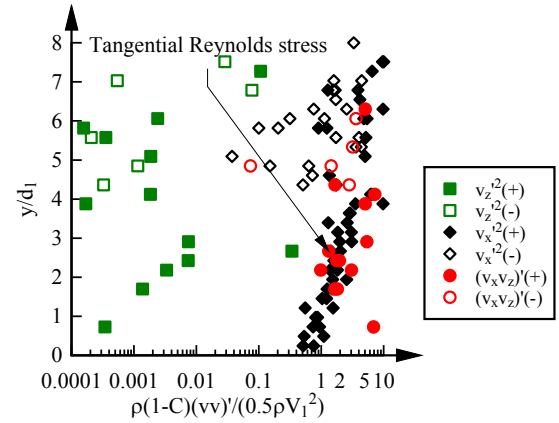

Figure 9: Normal and tangential Reynolds stresses.

7. Conclusion

Four-point air-water flow measurements were performed in hydraulic jumps using a phase-detection probe array consisting of two dual-tip probes. Velocity and turbulence properties were derived between any two probe sensor tips, including the characteristic transverse velocity and its fluctuations. The longitudinal velocity component was measured systematically with two opposite probe orientations in the shear flow and recirculation free-surface flow regions. The probe orientation had little impact on the time-averaged velocity measurement, but the probe support structures affected the velocity fluctuation quantification in the recirculation flow.

The characteristic instantaneous transverse velocity was derived based upon a number of small signal segments. Such a transverse velocity component was the result of a signal filtering for a given length scale (i.e. sensor separation distance) and a time scale (i.e. duration of signal segment). It provided a measure of the instantaneous transverse motion velocity in the bubbly flow. For a length scale $\sim 10^{-2}$ m and a time scale no larger than 0.2 s, the typical velocity of instantaneous transverse interface motions was estimated at 40% to 50% of the time-averaged longitudinal velocity. The corresponding transverse velocity fluctuations were one to two orders of magnitude smaller than the longitudinal turbulence intensity, with dimensionless transverse velocity fluctuations $v_z'/V_1 \sim 0.02$ to 0.5.

Although the direct measurement of turbulence intensity in a direction other than the longitudinal direction presented some scatter because of limitations of correlation analysis, the four-point sensor array enabled estimates of the normal and tangential Reynolds stresses in the highly aerated turbulent shear flow. Further investigations should be conducted in other air-water turbulent shear flows to ascertain the applications.

Acknowledgements

The authors thank Jason Van Der Gevel and Stewart Matthews (The University of Queensland) for their technical assistance in laboratory. The financial support of the Australian Research Council (Grant DP120100481) is acknowledged.

References

[1] Montes, S.J., *Hydraulics of Open Channel Flow*, ASCE Press, New York, 1998.

[2] Chanson, H., *Energy Dissipation in Hydraulic Structures*, IAHR Monograph, CRC Press, Taylor & Francis Group, Leiden, The Netherlands 2015.

[3] Hornung, H.G., Willert, C., and Turner, S., The flow field downstream of a hydraulic jump, *J. Fluid Mechanics*, 287, 299-316, 1995.

[4] Crowe, C., Sommerfield, M., and Tsuji, Y.,. *Multiphase Flows with Droplets and Particles*, CRC Press, Boca Raton, USA, 1998.

[5] Liu, M., Rajaratnam, N., and Zhu, D.Z., Turbulent structure of hydraulic jumps of low Froude numbers, *J. Hydraulic Engineering*, ASCE, 130(6), 511-520, 2004.

[6] Lennon, J.M., and Hill, D.F., Particle image velocity measurements of undular and hydraulic jumps, *J. Hydraulic Engineering*, ASCE, 132(12), 1283-1294, 2006.

[7] Mignot, E., and Cienfuegos, R., Energy dissipation and turbulent production in weak hydraulic jumps, *J. Hydraulic Engineering*, ASCE, 136(2), 116-121, 2010.

[8] Cartellier, A., Simultaneous void fraction measurement, bubble velocity, and size estimate using a single optical probe in gas-liquid two-phase flows, *Review of Scientific Instruments*, 63(11), 5442-5453, 1992.

[9] Chanson, H., Air-water flow measurements with intrusive, phase-detection probes: can we improve their interpretation?, *J. Hydraulic Engineering*, ASCE, 128(3), 252-255, 2002.

[10] Murzyn, F., Mouaze, D., and Chaplin, J.R., Air-water interface dynamic and free surface features in hydraulic jumps, *J. Hydraulic Research*, IAHR, 45(5), 679-685, 2007.

[11] Zhang, G., Wang, H., and Chanson, H., Turbulence and aeration in hydraulic jumps: free-surface fluctuation and integral turbulent scale measurements, *Environ Fluid Mechanics*, 13(2), 189-204, 2013 (DOI: 10.1007/s10652-012-9254-3).

[12] Wang, H., Felder, S., and Chanson, H., An experimental study of turbulent two-phase flow in hydraulic jumps and application of a triple decomposition technique, *Experiments in Fluids*, 55(7), Paper 1775, 18 pages & 2 video movies, 2014 (DOI: 10.1007/s00348-014-1775-8).

[13] Chanson, H., and Toombes, L., Air-water flows down stepped chutes: turbulence and flow structure observations, *Intl J. Multiphase Flow*, 28(11), 1737-1761, 2002.

[14] Felder, S., and Chanson, H., Triple decomposition technique in air–water flows: application to instationary flows on a stepped spillway, *International J. Multiphase Flow*, 58, 139-153, 2014 (DOI: 10.1016/j.ijmultiphaseflow.2013.09.006).

[15] Wang, H., and Chanson, H., Experimental study of turbulent fluctuations in hydraulic jumps, *J. Hydraulic Engineering*, ASCE, 141(7), Paper 04015010, 10 pages, 2015 (DOI: 10.1061/(ASCE)HY.1943-7900.0001010).

[16] Murzyn, F., and Chanson, H., Experimental investigation of bubbly flow and turbulence in hydraulic jumps, *Environ. Fluid Mechanic*, 9(2), 143-159, 2009 (DOI: 10.1007/s10652-008-9077-4).

[17] Chachereau, Y., and Chanson, H., Bubbly flow measurements in hydraulic jumps with small inflow Froude numbers, *Intl J. Multiphase Flow*, 37(6), 555-564, 2011 (DOI: 10.1016/j.ijmultiphaseflow.2011.03.012).

[18] Resch, F.J., and Leutheusser, H.J., Reynolds stress measurements in hydraulic jumps, *J. Hydraulic Research*, 10(4), 409-429, 1972.

[19] Chanson, H., Current Knowledge In Hydraulic Jumps And Related Phenomena. A Survey of Experimental Results, *European Journal of Mechanics B/Fluids*, 28(2), 191-210, 2009 (DOI: 10.1016/j.euromechflu.2008.06.004)

[20] Wang, H., and Chanson, H., Air Entrainment and Turbulent Fluctuations in Hydraulic Jumps, *Urban Water Journal*, 12(6), 502-518, 2015 (DOI: 10.1080/1573062X.2013.847464)